Scattering Suppression in a 4G and 5G Base Station Antenna Array Using Spiral Chokes

Journal:	*IEEE Antennas and Wireless Propagation Letters*
Manuscript ID	AWPL-07-20-1245.R1
Manuscript Type:	Original Manuscript
Date Submitted by the Author:	31-Jul-2020
Complete List of Authors:	Sun, Hai-Han; Nanyang Technological University Zhu, He; University of Technology Sydney Faculty of Engineering and Information Technology, Global Big Data Technologies Centre (GBDTC); University of Technology, Sydney Ding, Can; University of Technology Sydney, Jones, Bevan; University of Technology Sydney, Faculty of Engineering and IT Guo, Yingjie; University of Technology Sydney, GBDTC
Keywords:	base station antenna, choking techniques, cross-band scattering suppression, dual-band arrays

Response letter

Dear Editors and Reviewers,

Thank you for taking your time to review our revised paper and for your constructive comments to help us improve the quality of our manuscript. We have addressed all the comments made by the editors and reviewers in this round and revised the manuscript accordingly. Our point-to-point responses to the comments are listed below. The comments from editors and reviewers are copied in *blue* and our responses are in black. The revisions are marked in red in both the response letter and the revised manuscript.

Response to Associate Editor

One reviewer still has some comments and recommendations. Meanwhile, for the equivalent circuit of the spiral choke, the authors have shown the current on the spiral choke due to an impinging E field and compared to the current on the equivalent circuit, which look well-match.

(1) However, what is the voltage source used to drive the equivalent circuit that corresponds to the E field? Also, it seems that the authors did not provide other element values besides Lp and Cp, such as R, L1, C1, etc. Can they be omitted and are they nearly constant? What are their nominal values? The authors should at least provide in text the range of nominal values for these other circuit elements for the spiral parameters studied, e.g. R=10 ~ 20 ohm, L1= ..., C1= ... etc. Please also confirm whether the values are per-unit length (distributed as in replies) or lumped ones and take note of the correct units.

(2)The authors should address all these comments carefully and revise satisfactorily, taking into account proper font size, spacing, etc. (If the authors find that there is really insufficient space due to page limit, they may choose to submit to journal.)

Response: Thank you for your time reviewing our revised manuscript.

(1) To analyze the intrinsic property of the spiral structure, an infinite long spiral is simulated to eliminate the effects of discontinuities and to obtain general results that do not need to take account of the specific geometry of the antenna. The equivalent circuit model of the spiral can be simplified as a parallel RLC circuit, as shown in Fig. R1(a). A single cell of the spiral with periodic boundary conditions at both ends is modeled, as shown in Fig. R1(b). The periodic boundary is set to simulate an infinitely long spiral. The spiral is illuminated by a plane wave with E-field along the axis of the spiral with Ex = 1V/m. The current induced on the spiral and the voltage across one turn of the spiral are monitored, as shown in Fig. R1(b). The monitored current and voltage magnitudes are shown in Fig. R2.

For the circuit model, the current flowing through the circuit is calculated using

$$I_{calculated}(f) = \frac{V_{simulated}(f)}{Z(f)}$$

$$Z(f) = \frac{1}{\frac{1}{R} + \frac{1}{j2\pi fL} + j2\pi fC}$$

We did curve fitting for the magnitudes of the calculated current and the simulated current to extract the R, L, and C values. The result is shown in Fig. R3. The current magnitudes agree well with each other. The extracted R, L, and C values per millimeter are also listed in Fig. R3.

Using this method, the parameters for R, L, and C per millimeter are extracted for spirals with different parameters, as listed in Figs. 2 and 3 in the revised manuscript. We have updated Figs. 1-3 and revised the paragraph 2 and 3 in Section II accordingly in the revised manuscript.

(2) Thank you. We have addressed all of the comments we received in this round and revised the manuscript accordingly. We have adjusted the font size and spacing to improve the readability of the manuscript.

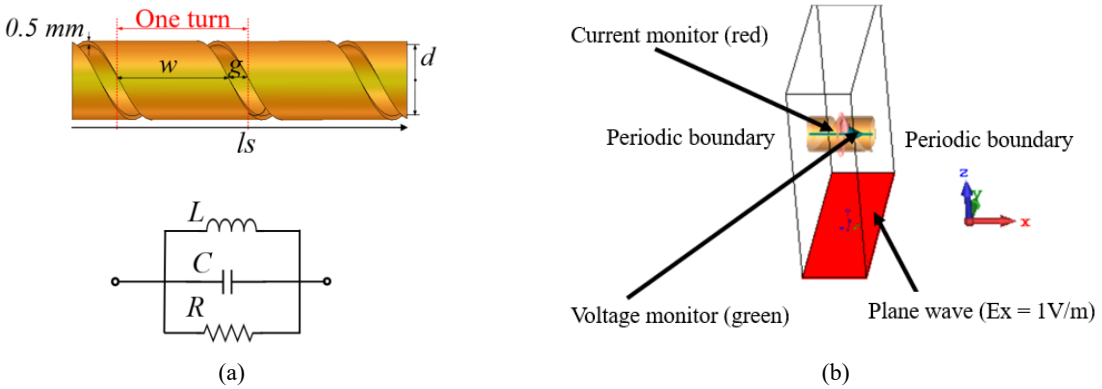

(a) (b)

Fig. 1. (a) Configuration of the spiral structure and the equivalent circuit model. (b) Demonstration of the spiral illuminated by a plane wave and the current and voltage monitors.

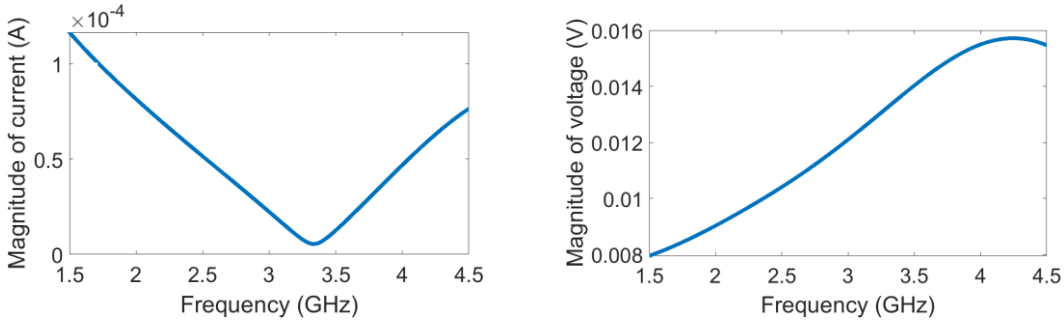

(a) (b)

Fig. R2. The magnitudes of (a) the monitored current, and (b) the monitored voltage.

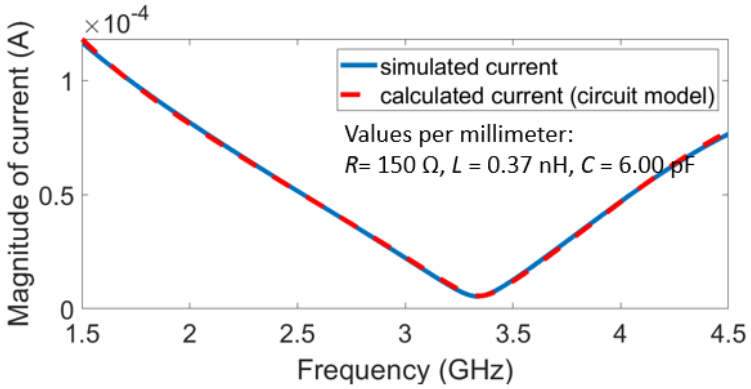

Fig. R3. A comparison of the magnitudes of the simulated current and the calculated current with the equivalent circuit.

Response to Reviewer 1

Regarding my concern about sidelobes in the HB, I didn't find a detailed reply from the authors on that and it doesn't appear to be tested in simulation. I see that the spacings now of the setup are 85mm and 65mm in the two axes of the plane. This corresponds to half wavelength spacings for frequencies of 1.7GHz and 2.3GHz respectively, well below the HB of 3.4-3.8GHz that it really focuses on. So at 3.5GHz, the half wavelength spacing is 42mm, much less, and so with the setup we have, 1 wavelength and 0.75 wavelength spacings approximately. This is going to definitely cause grating lobes and isn't good for massive MIMO type setups. However, if this is for small cell base stations, it will still yield enough de-correlation for the MIMO coding used there and the LB antenna also will have 85mm spacing and hence has enough de-correlation and de-coupling. Therefore I recommend that the authors

put in to say that this setup gives minimum half wavelength spacing at all frequencies for de-correlation in small cell MIMO antennas.

Response: Thank you for your suggestion. Yes, the spacings of the HB elements result in a slightly large sidelobe level at high frequencies. The normalized radiation patterns of the HB sub-array I in the *yz*-plane at 3.3 GHz, 3.5 GHz, and 3.7 GHz are shown in Fig. R4. The sidelobe levels are -17.9 dB, -15.4 dB, and -12.7 dB, respectively. As the HB sub-arrays I and II are designed to operate separately, their radiation is not combined. Instead, a spacing of 85 mm (a wavelength at 3.5 GHz) guarantees high isolation between the two HB sub-arrays. The reviewer is correct in saying that this setup guarantees the minimum half-wavelength spacing at all frequencies for de-correlation when used in small cell base stations. We have revised the first paragraph in Section III to clarify the issue:

"… The two HB columns form two HB sub-arrays for multiple-input and multiple-output (MIMO) application. The LB and HB antennas are designed to operate from 1.71 GHz to 2.2 GHz, and from 3.3 GHz to 3.7 GHz for the 4G and 5G operations, respectively. The spacings between HB elements in the array gives a minimum half-wavelength spacing at all frequencies for de-correlation in small cell MIMO antennas. …"

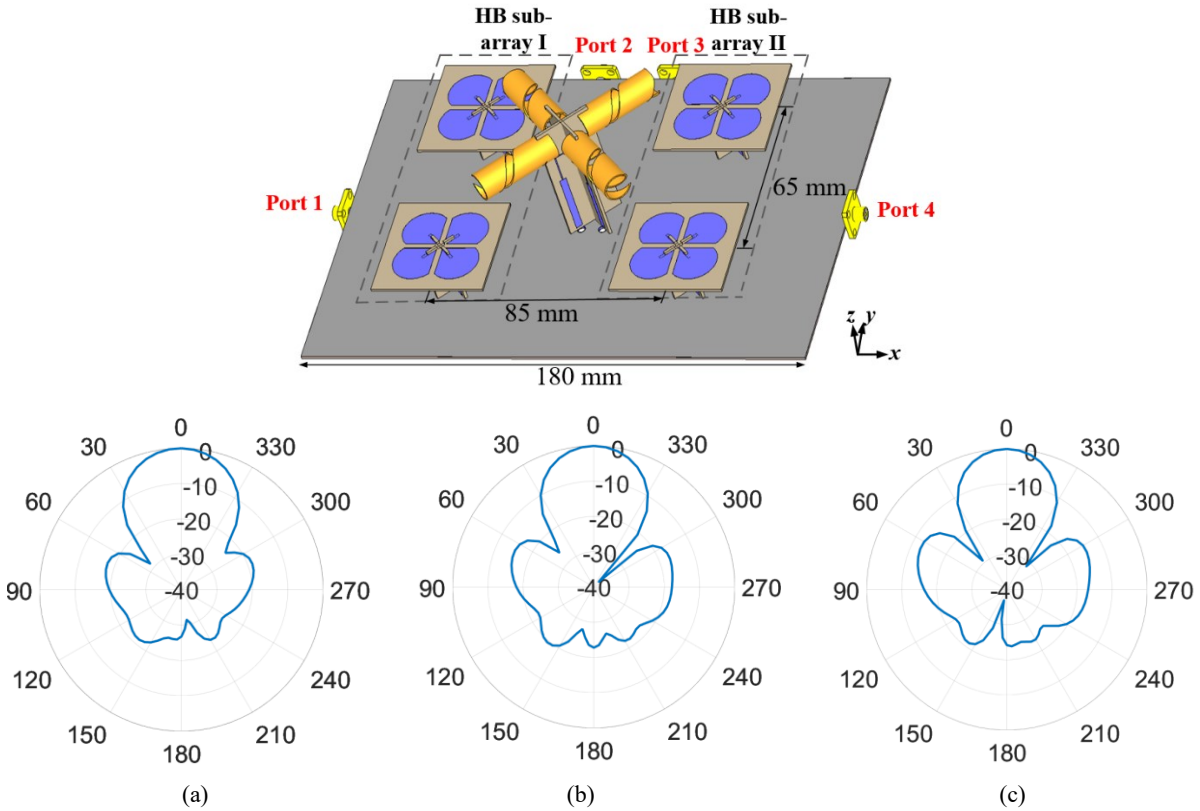

Fig. R4 The normalized radiation patterns of the HB sub-array I in the *yz*-plane at (a) 3.3 GHz, (b) 3.5 GHz, and (c) 3.7 GHz.

Also another minor correction I recommend is to consider the unit of Amps used in the revised current plots. I would recommend uA (or Micro amps) since then it is comparing tens of micro Amps and hundreds or thousands of micro Amps that should make easier comparison.

Response: Thank you for the very good suggestion. We have modified the figures and used the current unit μA in Figs. 2 and 3 for the ease of comparison.

Scattering Suppression in a 4G and 5G Base Station Antenna Array Using Spiral Chokes

Hai-Han Sun, *Member, IEEE,* He Zhu, *Member, IEEE*, Can Ding, *Member, IEEE*, Bevan Jones, *Life Member, IEEE*, and Y. Jay Guo, *Fellow, IEEE*

***Abstract*— This paper presents a novel distributed choking technique, the spiral choke, for scattering suppression in dual-band antenna arrays. The working principle and the scattering suppression capability of the choke are analyzed. The spiral chokes are implemented as low-band radiators in a co-located 4G and 5G dual-band array to suppress cross-band scattering while broadening the bandwidth of the choked element. The experimental results demonstrate that the cross-band scattering in the array is largely eliminated, and the realized dual-band array has very stable radiation performance in both well-matched bands.**

***Index Terms*— base station antennas, 4G, 5G, choking techniques, cross-band scattering suppression, dual-band arrays**

I. Introduction

Nowadays, there is a concerted international effort to deploy the fifth-generation (5G) mobile communications networks. Owing to environmental and cost considerations, mobile operators expect 5G antenna arrays to be collocated to fourth-generation (4G) ones on the same panels, whilst no major degradation of antenna radiation patterns is allowed. However, the close spacing between elements at different bands often leads to strong cross-band scattering. Especially, elements operating in the low band (LB) usually present as large scatterers in the high band (HB), causing the distortion of HB radiation patterns and the reduction of the cross-band port isolation. The cross-band scattering problem has been a long-existing issue in multi-band antenna arrays.

To suppress the cross-band scattering, the traditional method uses a variety of metal baffles or walls [1]-[4]. The shape, size, and position of metal baffles are optimized through trial and error to improve the radiation performance in both bands. Some reduction in cross-band scattering can be achieved, but the method adds design complexity especially when several different bands are involved.

Choking techniques have been presented to suppress cross-band scattering in dual-band interleaved arrays [5], [6]. Instead of modifying the surrounding environment, this method modifies the LB radiator by inserting lumped chokes with LB-pass HB-stop property. This method minimizes the unwanted HB currents on LB arms and restores the HB radiation patterns. In [6], a dual-band array with choked LB element achieves low scattering and uncontaminated radiation performance in both bands. However, the inserted lumped chokes make the impedance matching of the choked antenna difficult. The achieved impedance bandwidth of the choked antenna is only 19.7% with $|S_{11}| < -10$ dB, which still fall short of the industrial requirements. Further investigations on the choking technique are therefore needed to improve the bandwidth of the choked elements while having a good scattering suppression capability.

In this paper, we present a novel distributed choking structure, the spiral choke, as LB radiators to suppress HB scattering and broaden the bandwidth of choked LB antenna. The spiral structure has its intrinsic choking capability in the high band and operates like a dipole radiator in the low band, thus has negligible effects on the HB radiation while maintaining good matching capability in the low band. The spiral-choked LB element is employed in an interleaved 4G and 5G BSA array to demonstrate its performance. The array covers the 4G band from 1.71 GHz to 2.26 GHz, and the 5G band from 3.3 GHz to 3.7 GHz with excellent matching capability ($|S_{11}| <$ -15 dB). With the spiral LB element implemented, the array achieves clean patterns with half-power beamwidth (HPBW) variation of 65°±5° in both the high and low bands. The array features a simple structure thus simplifying the design and manufacture. It also demonstrates a practical solution to the current industrial problem of co-locating 4G and 5G antennas.

II. The Spiral Choke

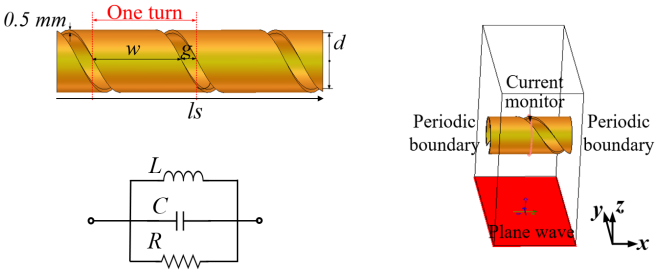

Fig. 1. (a) Configuration of the spiral structure and the equivalent circuit model. (b) Demonstration of the spiral illuminated by plane wave.

The configuration of the spiral structure is presented in Fig. 1(a). Similar to the helix coil, each cell of the spiral can be represented as a parallel *RLC* circuit. It acts as an open circuit at its resonant frequency where the impedance of the spiral goes to infinity, so an incident electric-field (E-field) cannot induce longitudinal currents. In the frequency bands that are much lower than the resonant point, the circuit has a lower inductive impedance and a higher shunt capacitive impedance. It only introduces an additional small inductance compared with the corresponding cylindrical conductor, thus has a minimal effect on the radiator's impedance. The intrinsic property of the spiral makes it a distributed choke, which can be used as a LB radiator

Manuscript submitted on July 07, 2020 and revised on July 30, 2020.

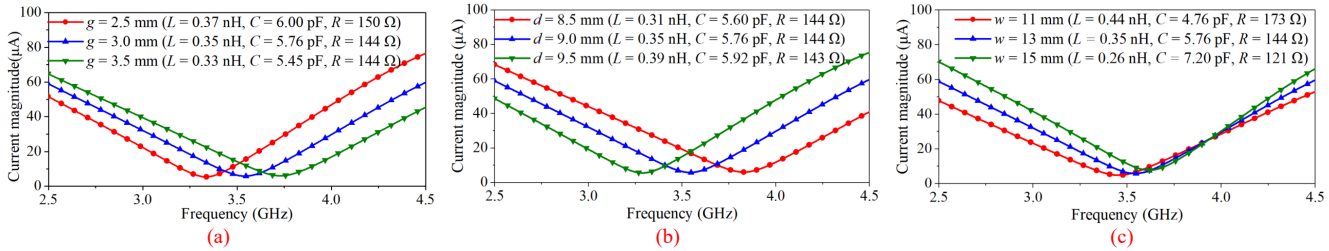

Fig. 2. Magnitude of the induced currents on the spiral structure with different values of (a) gap g, (b) inner diameter d, and (c) width of strip w. Other parameters of the spiral are g = 3.0 mm, d = 9.0 mm, and w = 13.0 mm unless specified in the plots. The thickness of the conductor is 0.5 mm.

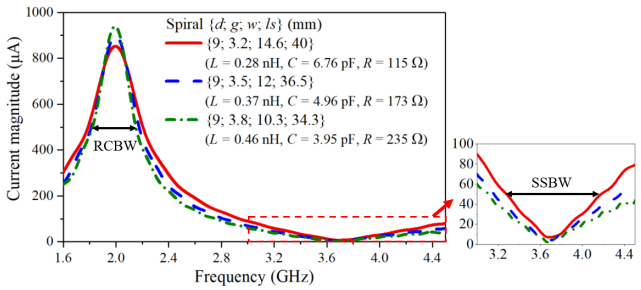

Fig. 3. Magnitude of the induced currents on the finite-length spiral structure that has an open-circuit resonance at 3.7 GHz and a short-circuit resonance at 2.0 GHz with different combinations of parameters.

to suppress the unwanted induced HB currents while maintaining the radiating currents in the low band.

To study the ability of the spiral to suppress the HB currents, we need to find the resonant point of the spiral, which is the frequency where currents induced by an incident E-field are minimized. Minimizing induced HB currents on the spiral minimizes the HB scattering. To achieve this, a single cell of the spiral with periodic boundary conditions at both ends is modeled, as shown in Fig. 1(b). It is illuminated by a plane wave with E-field along the axis of the spiral (x-axis), and currents induced on it are monitored. The periodic boundary is set to simulate infinitely long spiral to eliminate the effects of discontinuities and allows us to obtain general results that do not need to take account of the specific geometry of the HB and LB elements.

There are three important parameters for tuning the resonant frequency of the spiral: the distance between neighboring turns g, the inner diameter of spiral d, and the width of strip w. The induced currents flowing on the spiral structure with different values of g, d, and w are monitored and plotted in Fig. 2. The approximate values of distributed circuit components per millimeter of the spiral in different cases are extracted. They are also listed in the figures. As shown in Fig. 2(a), a larger g moves the minimum current point to a higher frequency, corresponding to the spiral's resonant point moving to a higher frequency. This is because increasing g decreases both L and C, which in turn raises the parallel resonant frequency. Fig. 2(b) shows a larger d moves the resonant point to a lower frequency, as it increases both L and C. Fig. 2(c) shows a larger w moves the resonant point to a higher frequency, as it largely decreases L and only increases C to a smaller amount.

The spiral is implemented as LB radiators to suppress scattering currents in the high band, while maintaining radiating currents in the low band. To examine its performance in high and low bands with different combination of parameters, we selected several finite-length spirals with an intrinsic open-circuit resonance at 3.7 GHz and a half-wavelength short-circuit resonance at 2.0 GHz, and compared the magnitudes of induced currents on them, as shown in Fig. 3. Here we define the HB scattering suppression bandwidth (SSBW) and the LB radiating current bandwidth (RCBW) as the band in which magnitude of current is less than 50 μA and higher than 500 μA, respectively. Fig. 3 shows that a spiral with larger g and smaller w has a wider SSBW but has a slightly narrower RCBW. The spiral with a larger g and a smaller w has a smaller C and a larger L per unit length. Therefore, it is concluded that a larger L/C enhances the HB SSBW but reduces the LB RCBW. The optimization criteria of the spiral chokes as LB radiators are to effectively suppress the cross-band scattering in the high band while maintaining good matching and radiation performance in the low band.

III. Implementation of the Spiral Choke in an Interleaved 4G and 5G Dual-Band Antenna Array

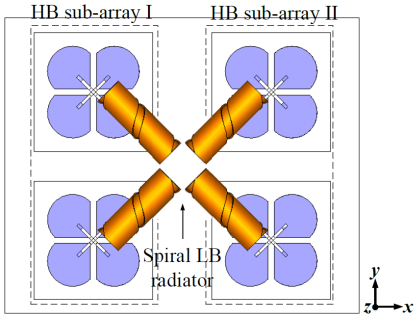

Fig. 4. Arrangement of the interleaved dual-band array with spiral LB radiators.

The spiral choking structure is implemented as LB radiators in a compact dual-band antenna array section to verify its HB scattering suppression performance, as shown in Fig. 4. Both the LB and HB radiators have the cross-dipole arrangement [8]-[10] for the required dual-polarized radiation for base station applications. The LB element is located midway between the HB elements in two columns. The two HB columns form two HB sub-arrays for multiple-input and multiple-output (MIMO) application. The LB and HB antennas are designed to operate from 1.71 GHz to 2.2 GHz, and from 3.3 GHz to 3.7 GHz for the 4G and 5G operations, respectively. The spacings between HB elements in the designed array gives

a minimum half-wavelength spacing at all frequencies for de-correlation in small cell MIMO antennas. In order to more effectively suppress scattering currents in the high band, the parameters of the spirals in this design are optimized to have a resonant point at 3.7 GHz as the distortion of HB patterns caused by the presence of unmodified LB element (cylindrical LB element) is more severe at frequencies around 3.7 GHz. The optimized parameters are $d = 9$ mm, $w = 14.1$ mm, and $g = 3.23$ mm.

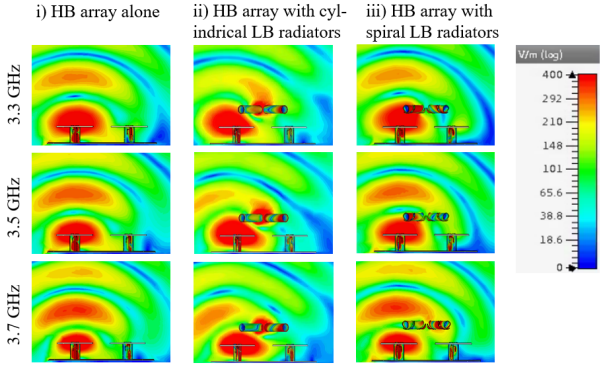

Fig. 5. The electric-field cuts in the *xz*-plane under the circumstances of i) HB array alone, ii) HB array with cylindrical LB radiators, and iii) HB array with spiral LB radiators.

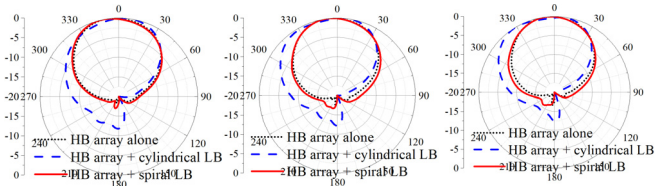

Fig. 6. Comparison of normalized HB radiation pattern in the horizontal plane (*xz*-plane) under the circumstances of i) only HB array, ii) HB array with cylindrical LB radiators, and iii) HB array with spiral LB radiators at (a) 3.4 GHz, (b) 3.6 GHz, (c) 3.7 GHz.

To examine the spiral's capability in suppressing the HB scattering, the E-field distribution and the radiation pattern with one of the HB sub-arrays being excited are investigated. The results are shown in Figs. 5 and 6. At this stage, LB feed networks are not included to eliminate their influence. Subsequent simulations show that LB feeding networks only have little effect on HB radiation performance. Fig. 5 shows the E-field distributions in the horizontal section through the array in three cases: i) HB array alone, ii) HB array with cylindrical LB arms, and iii) HB array with spiral LB arms. Compared with the E-field when only HB array is present, cylindrical LB radiators block the HB E-field to a large extent. The spiral LB radiators have much less effect on the HB E-field. The resultant horizontal patterns in these three cases from 3.3 GHz to 3.7 GHz are shown in Fig. 6. The deterioration of the HB radiation patterns in the presence of the cylindrical LB radiators (unmodified LB radiators) has been largely eliminated using spiral LB arms, demonstrating the effectiveness of the spiral structure in reducing HB pattern distortion.

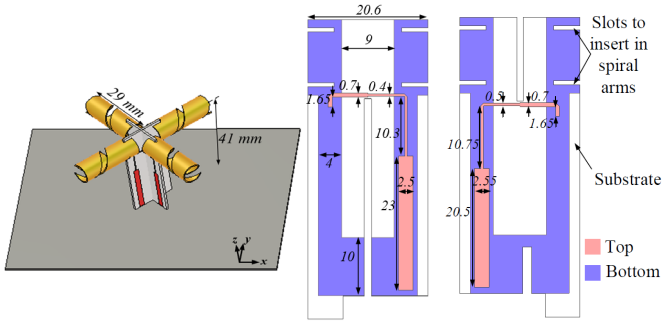

Fig. 7. (a) Perspective view of the spiral LB element. (b) Configurations of the two baluns for the spiral LB element. (The substrate is FR4 with dielectric constant of 4.4, and a thickness of 1.0 mm.)

After demonstrating the effectiveness of the spiral structure in suppressing the cross-band scattering, the spiral radiators are matched and balanced fed by baluns in the low band. The baluns are designed following the guidelines in [11], [12]. Two baluns are orthogonally arranged to feed the two pairs of spiral arms. The final configuration of the spiral LB antenna is shown in Fig. 7. The spiral antenna is well-matched with reflection coefficients <-15 dB from 1.66 GHz to 2.22 GHz. The radiation patterns of the spiral element are very stable across the band.

IV. Experimental Results of the Dual-Band Array

The configuration of the finalized dual-band array section is shown in Figs. 8 (a) and 8(b). The distance between the two HB sub-arrays is set as 1λ at 3.5 GHz to guarantee good isolation. The HB sub-arrays are fed by power dividers printed on the back of the reflector, and the LB element is fed by coaxial cables directly connected to the LB baluns. The array has been fabricated and tested, as shown in Fig. 8(c).

The S-parameters of the HB ports are shown in Fig. 9. Figs.

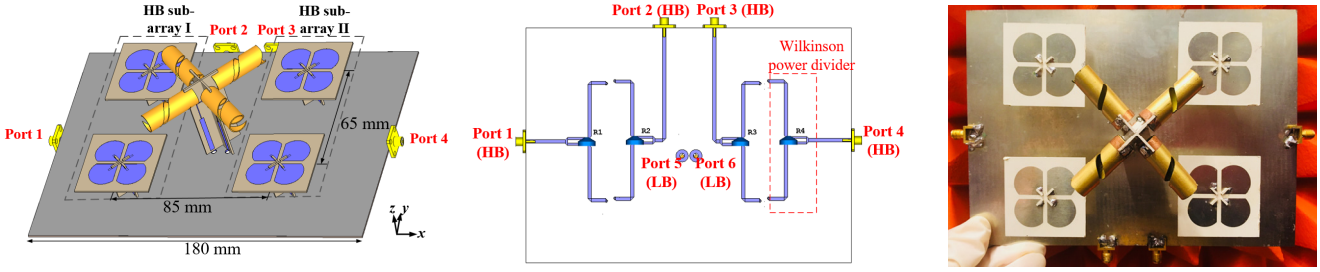

Fig. 8. (a) Perspective view of the dual-band antenna array model. (b) View of the feed network for the dual-band antenna array. (c) Front view of the fabricated antenna array prototype.

9(a) and 9(b) show the reflection coefficients and isolations, respectively. The measured bandwidth is 11.4% from 3.3 GHz to 3.7 GHz for reflection coefficients < -15 dB. The isolations between ports in the same sub-array and in different sub-arrays are all > 25 dB. The HB radiation patterns are plotted in Fig. 10. The +45°-polarized patterns for sub-array I are presented. The results for −45° polarization and for sub-array II are almost identical with the presented results due to the symmetric geometry of the array configuration. The measured cross-polarization level is < −17 dB at the boresight. The radiation patterns are stable across the operating band with HPBWs of 66.5°±3.5°, which is shown in Fig. 11(a). Fig. 11(b) shows that the measured gain of the HB sub-array is around 11 dBi, which is 0.5 dBi less than the simulated one. This is attributed to the losses in the SMA terminators and cables for measurement.

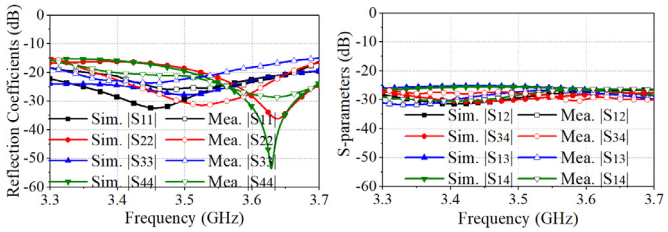

(a) (b)

Fig. 9. Simulated and measured (a) reflection coefficients and (b) isolations for HB ports.

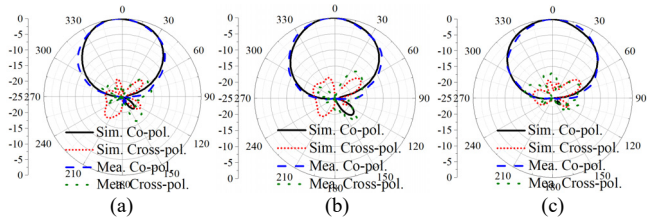

(a) (b) (c)

Fig. 10. Normalized simulated and measured horizontal radiation patterns for the HB antennas at (a) 3.3 GHz, (b) 3.5 GHz, and (c) 3.7 GHz.

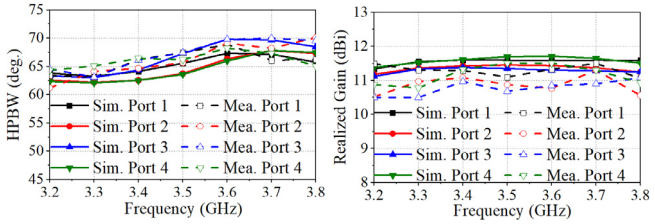

(a) (b)

Fig. 11. Simulated and measured (a) HPBW, and (b) gain for HB sub-arrays.

The results for the spiral LB element are shown in Figs. 12 - 14. Fig. 12 plots the reflection coefficients and isolation results. The measured bandwidth is 28.3% from 1.7 GHz to 2.26 GHz for reflection coefficients <−15 dB. The isolation between orthogonal ports is > 22 dB across the band, which is slightly lower than most of the cross-dipole antennas due to the coupled currents along slots in the spiral arms. Fig. 13 shows the LB radiation patterns of the +45° polarized radiation. The cross-polarization level is < -17 dB at the boresight. The horizontal HPBW and gain of the LB element are plotted in Fig. 14. The LB radiation patterns are consistent with HPBWs of 65°±5°. The simulated and measured gains are around 8 dBi and 7 dBi, respectively. The difference can be caused by the loss of the coaxial cables, and FR4 substrates of the baluns.

The implementation of spiral-choked LB element also improves the cross-band isolation in the high band but has negligible impact on the isolation in the low band. The co-polarized and cross-polarized cross-band isolation in the high band is improved from -18 dB to -22 dB, and from -21 dB to -26 dB, respectively.

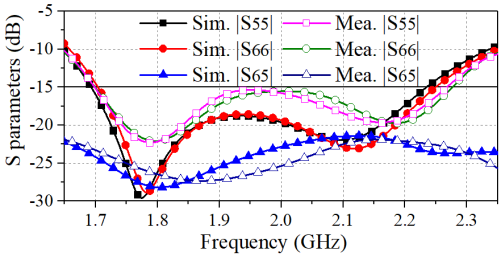

Fig. 12. Simulated and measured S-parameters for the spiral LB antenna.

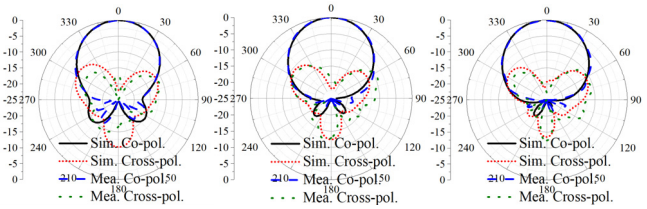

(a) (b) (c)

Fig. 13. Normalized simulated and measured +45°-polarized horizontal radiation patterns for the spiral LB antenna at (a) 1.7 GHz, (b) 1.9 GHz, and (c) 2.2GHz.

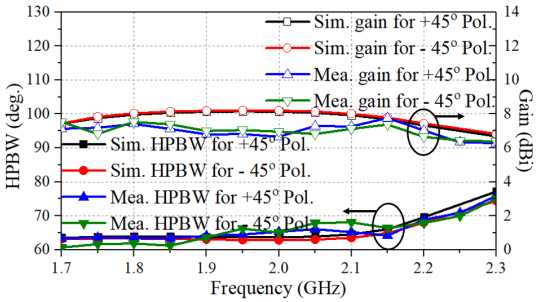

Fig. 14. Simulated and measured HPBW and gain for the spiral LB antenna.

V. Conclusion

In this paper, a novel distributed choke, the spiral choke, is implemented in an interleaved 4G and 5G BSA array to minimize cross-band scattering. As a distributed choking structure, the spiral has intrinsic scattering suppression capability and helps to broaden the bandwidth of the choked LB antenna. The experimental results of the dual-band array demonstrate that the distortion of the HB pattern caused by the scattering from the cylindrical LB element is largely corrected with the spiral chokes. The spiral-choked LB element has a wider bandwidth with a better matching capability than the one in the previous work [6]. The presented dual-band array achieves stable radiation properties across well-matched high and low bands with a very simple and compact structure, which makes it highly suitable for the use in 4G and 5G BSA systems.

REFERENCES

[1] H. Huang, Y. Liu, and S. Gong, "A novel dual-broadband and dual-polarized antenna for 2G/3G/LTE base stations," *IEEE Trans. Antennas Propag*., vol. 64, no. 9, pp. 4113-4118, Sep. 2016.

[2] H. Huang, Y. Liu, and S. Gong, "A dual-broadband dual-polarized base station antenna for 2G/3G/4G applications," *IEEE Antennas Wirel. Propag. Lett*., vol. 16, pp. 1111-1114, 2017.

[3] Y. He, Z. Pan, X. Cheng, Y. He, J. Qiao, M. M. Tentzeris, "A novel dual-band dual-polarized miniaturized and low-profile base station antenna", *IEEE Trans. Antennas Propag*., vol. 63, no. 12, pp. 5399-5408, Dec. 2015.

[4] Y. He, W. Tian, L. Zhang, "A novel dual-broadband dual-polarized electrical downtilt base station antenna for 2G/3G applications", *IEEE Access*, vol. 5, pp. 15241-15249, June 2017.

[5] B. Jones, O. Isik, and C. Shang, "Dual-band interspersed cellular basestation antennas," *EP. Patent 2 769 476 B1*, Dec. 24, 2012.

[6] H. H. Sun, C. Ding, H. Zhu, B. Jones, and Y. J. Guo, "Suppression of cross-band scattering in multiband antenna arrays," *IEEE Trans. Antennas Propag*., vol. 67, no. 4, pp. 2379-2389, Apr. 2019.

[7] D. Su, D. Fu, T. N. C. Wang, and H. Yang, "Broadband polarization diversity base station antenna for 3G communication system," *J. of Electromag. Waves and Appl*., vol. 22, pp. 493 – 500, 2008.

[8] H. Huang, Y. Liu, and S. Gong, "A broadband dual-polarized base station antenna with sturdy construction," *IEEE Antennas Wirel. Propag. Lett*., vol. 16, pp. 665 – 668, Mar. 2017.

[9] Y. Cui, R. Li, and H. Fu, "A broadband dual-polarized planar antenna for 2G/3G/LTE base stations," *IEEE Trans. Antennas Propag.*, vol. 62, no. 9, pp. 4836 - 4840, Sep. 2014.

[10] W. K. Roberts, "A new wide-band balun," *Proc. IRE,* vol. 45, pp. 1628 – 1631, Dec. 1957.

[11] H. Sun, C. Ding, B. Jones and Y. J. Guo, "A wideband base station antenna element with stable radiation pattern and reduced beam squint," IEEE Access, vol. 5, pp. 23022–23031, Oct. 2017.